Tetrahedron 64 (2008) 10874–10881

Contents lists available at ScienceDirect

Tetrahedron

journal homepage: www.elsevier.com/locate/tet

Synthesis and conformational studies of chiral *meso*-(α,β-unsaturated)-porphyrins

Alexandra Fateeva, Adrian Calborean, Jacques Pécaut, Pascale Maldivi, Jean-Claude Marchon, Lionel Dubois *

Laboratory of Inorganic and Biological Chemistry, UMR_E 3 (CEA-University J. Fourier), CEA, INAC, SCIB, RICC, 17 rue des Martyrs, F-38054 Grenoble, France

ARTICLE INFO

Article history:
Received 5 June 2008
Received in revised form 2 September 2008
Accepted 3 September 2008
Available online 17 September 2008

Keywords:
Porphyrins
Atropoisomers
Variable temperature NMR

ABSTRACT

We describe a method to improve the yield and the kinetics of the difficult syntheses of α,β-unsaturated porphyrins, which enabled us to obtain a new chiral porphyrin derived from (*S*)-(−)-perillaldehyde in a 6% yield. Variable temperature NMR experiments on the free base, the zinc(II) and the nickel(II) complexes showed that two distinct and consecutive dynamic processes linked with the *meso* substituents rotation occurred. These processes can be analyzed as an evolution of the conformer composition upon temperature change. Higher values are found for the free energies of rotation of the substituent (measured by variable temperature ^{1}H NMR) compared to those of other equivalent porphyrins like *meso*-tetraphenyl porphyrin or *meso*-tetracyclohexyl porphyrin.

© 2008 Elsevier Ltd. All rights reserved.

1. Introduction

Numerous *meso*-substituted porphyrins have been studied until now, and in this family tetraphenyl porphyrin (**TPP**) plays a pivotal role for the characterization and the reactivity studies of metalloporphyrins. On the other hand with its fully hydrogenated substituents, tetracyclohexyl porphyrin (**TChP**) possesses particular steric and electronic features. Porphyrins bearing cyclic α,β-unsaturated substituents could be seen as intermediates between **TPP** and **TChP**, but in fact this family has its own features, distinct from **TPP** and **TChP**, especially on the dynamic stereochemistry point of view. This point is of particular importance for their catalytic properties.[1–3] For *meso* α,β-unsaturated porphyrin family, only tetramyrtenyl porphyrin (**H_2MyrtP**) were partly studied in the past. This can be explained by their difficult synthesis.[4,5] In this paper we report in detail the synthesis of new chiral *meso* α,β-unsaturated porphyrins derived from (*S*)-(−)-perillaldehyde (**H_2PeriP**, Scheme 1) and the X-ray structure of its nickel(II) complex. We also describe the dynamic stereochemistry of its free base, zinc(II) and nickel(II) complexes and we complete the studies on the free base and the zinc(II) complex of the tetramyrtenyl porphyrin started earlier in the laboratory.[4] Finally, some theoretical calculations of the activation rotation energy for the *meso* substituent helped us to have a better understanding of the dynamic behaviour of these porphyrins.

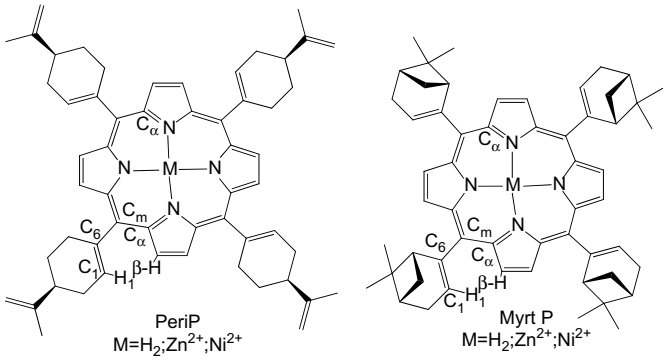

Scheme 1. Drawing of the porphyrin.

2. Results

2.1. Synthesis

Only a few number of α,β-unsaturated porphyrins have been synthesized and characterized to date.[4,6–13] Due to a good synthetic yield (11%), only myrtenal based porphyrins were investigated earlier.[4] Preliminary results obtained in our laboratory showed that

* Corresponding author. Tel.: +33 4 38 78 92 57; fax: +33 4 38 78 50 90.
E-mail address: lionel.dubois@cea.fr (L. Dubois).

0040-4020/$ – see front matter © 2008 Elsevier Ltd. All rights reserved.
doi:10.1016/j.tet.2008.09.009

no detectable amount of porphyrin is obtained with (*S*)-(−)-perillaldehyde as starting material, so we decided to test other conditions to synthesise **H_2PeriP**. We started from the Lindsey's protocol,[14] i.e., high dilution, a chlorinated solvent and an acidic catalyst followed by a DDQ oxidation of the porphyrinogen to porphyrin. The maximum yield was measured by UV–vis analysis, after DDQ oxidation, of small aliquot taken from time to time. Results obtained during the various tests are collected in Table 1 of Supplementary data. The best solvent for this synthesis is chloroform. As catalyst 1 equiv of TFA gives a better yield than $BF_3 \cdot Et_2O$. As for other porphyrins, the best concentration of reactive chemicals is 10^{-2} M. Yield is increased by using an excess of aldehyde toward pyrrole, thus a two or threefold excess of aldehyde seems to be an optimum. Under these conditions, after 30 h of reaction, the yield is around 4.5%. In the same conditions the **H_2MyrtP** yield is improved to 17%. By using the 1,3-dioxolane derived from (*S*)-(−)-perillaldehyde as a starting material in the best conditions described before, results showed a slightly higher yield (6% for **H_2PeriP**) and a shorter reaction time (6 h). To our knowledge, only one example of synthesis of *meso* α,β unsaturated porphyrin starting from the protected acetal form is described. Is this case, the authors advocated the use of α,β-unsaturated seleno-acetal to obtain good porphyrins yields.[15] Nevertheless the synthesis of the starting seleno-acetal is much more difficult compared to the simple dioxolanes we used.

We also made some tests with other α,β-unsaturated aldehydes: 1-cyclohexene-1-carboxaldehyde and 1-cyclopentene-1-carboxaldehyde. 1-Cyclohexene-1-carboxaldehyde gives no detectable amounts of porphyrin, whereas a yield of 2% was obtained by starting from the 1,3-dioxolane. Using 1-cyclopentene-1-carboxaldehyde, no amount of porphyrin was detected in any case. Thus, we focused our studies on **MyrtP** and **PeriP**.

2.2. Characterizations

2.2.1. Solid state characterization

2.2.1.1. X-ray diffraction. **NiPeriP** crystallizes in a *I*4(1) space group. A summary of crystallographic data is shown in Table 1. Its structure is represented in Figure 1. For an isolated porphyrin, the Ni^{2+} ion is located on a C_2 axis perpendicular to the porphyrin core. Thus, only two independent substituents are observed, one of them possessing a higher disorder. A substituent can have only two orientations: with H_1 directed upward or downward the mean porphyrin plane (Scheme 2). Thus, due to the perpendicular C_2 axis, only atropoisomers αααα and αβαβ can exist in the crystal. If we compare these two atropoisomers, they possess two identical substituents and two of the opposite conformation. Consequently in the solid state this mixture of atropoisomers will shown one substituent well defined and an other with a higher disorder. So, accordingly with the structure it is possible to postulate that two atropoisomers αααα and αβαβ, randomly distributed within the crystal, exist in the solid state.

Table 1
Crystallographic data for **NiPeriP**

Empirical formula	$C_{56}H_{60}N_4Ni$
Formula weight	847.79
Temperature	100(2) K
Wavelength	1.54184 Å
Crystal system	Tetragonal
Space group	*I*4(1)
Unit cell dimensions	a=16.7810(10) Å; α=90° b=16.7793(10) Å; β=90° c=15.5432(9) Å; γ=90°
Volume	4376.5(4) Å^3
Z	4
Density (calculated)	1.287 g/cm^3
Absorption coefficient	0.962 mm^{-1}
Completeness to θ=66.50°	98.70%
Final R indices [$>2\sigma(I)$]	R_1=0.0471, wR_2=0.1338
Final R indices (all data)	R_1=0.0607, wR_2=0.1445
Largest diff. peak and hole	0.299 and −0.217 e/Å^3
Flack parameter	0.11(8)

The mean plane of the cyclohexene substituent is tilted by about 80° toward the porphyrin mean plane. On the structure established at the Cu Kα wavelength, a Flack parameter of 0.11(8) enables unequivocal assignment of the structures chirality. The chiral carbon bearing the isopropen moiety possesses an (*S*) absolute configuration, as observed in the starting (*S*)-(−)-perillaldehyde.

Concerning the porphyrin core, the length of the Ni–N bond (1.944(5) Å) is in the upper range compared to other Ni^{2+} porphyrins described in the literature.[16–18] **NiPeriP** possesses a slightly non-planar porphyrin core, the mean dihedral angle between C_α–N–N–C_α (both N belonging to opposite pyrroles rings, the two C_α being in cis position on the opposite pyrroles, see Scheme 1) is 12°, and the angles between N–Ni–N are 176.3(5)° and 175.8(4)°. Due to the symmetry, two values for the N–C_α–C_m–C_α angles are found: one around 0.5° and the other around 9.0°. Pyrrole rings are quite flat as the dihedral angles between N–C_α–C_β–C_β are below 3.4°. It is interesting to compare these values with those described in the literature for **NiMyrtP**, **NiTPP** and **NiTChP**[17] since these molecules possess also C6 rings as *meso* substituents. For these porphyrins a shorter Ni–N bond is observed (1.902 Å for **NiMyrtP**, 1.931 Å for **NiTPP** and 1.8875 Å for **NiTChP**) corresponding to a more distorted core (C_α–N–N–C_α=43° and N–Ni–N=179° for **NiMyrtP**, C_α–N–N–C_α=27° and N–Ni–N=179° for **NiTPP**; C_α–N–N–C_α=47° and N–Ni–N=178° for **NiTChP**). To go further into the analysis of the core distortion, we used the NSD deconvolution program developed by Shelnutt et al.[19] The results obtained are given in Figure 2. They show that the distortion of **NiPeriP** mainly occurs in the saddled mode with an important contribution of the ruffled mode, contrary to **NiMyrtP**, **NiTChP** and **NiTPP**, which are mostly twisted in the ruffled mode.

2.2.2. Characterizations in solution

2.2.2.1. UV–vis spectroscopy. In a general way, the Soret band is lower in energy with **MyrtP** than with **PeriP**. This can be related to the porphyrin core distortion.[20] Thus the red-shift of the Soret band in **MyrtP** can lie in a more distorted core, confirming in solution the assessment made from the X-ray structure for the nickel complexes.

2.2.2.2. NMR spectroscopy. At room temperature, ^{1}H NMR spectra of all the studied porphyrins are quite broad. NMR spectra (^{1}H and ^{13}C) corresponding to the synthesized porphyrins were attributed by using 2D NMR experiments as COSY, NOESY or HSQC. Selected proton chemical shifts are given in Table 2. At room temperature, β-pyrrolic protons (β-H) have chemical shifts in the range from 9.2 to 9.7 ppm, and the proton of the double bond of the *meso* substituent H_1 has chemical shift between 6.3 and 6.7 ppm. For free base porphyrins, N–H proton chemical shifts are lower (−2.99 ppm) for **H_2PeriP** than for **H_2MyrtP** (−2.70 ppm). This is known to be due to a higher cyclic current and consequently to a less twisted porphyrin core. This result corroborates the observation that in solution, as in the solid state for the nickel complexes, **H_2PeriP** is less distorted than **H_2MyrtP**. For a same family, **PeriP** or **MyrtP**, β-H chemical shifts are easy to correlate to the porphyrin distortion. A highly twisted core gives rise to a lower cyclic current, which leads to lower β-H chemical shifts. Therefore, we can propose that the porphyrin distortion follows the order **NiPeriP**>**H_2PeriP**>**ZnPeriP**.

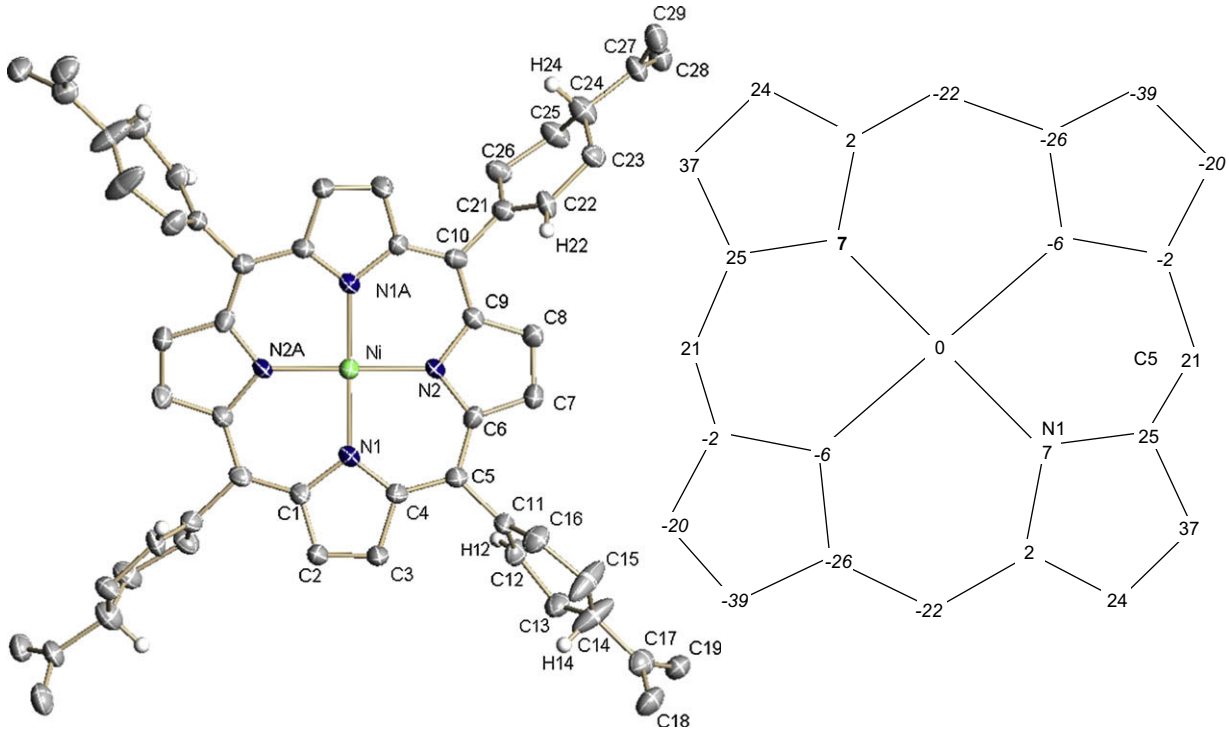

Figure 1. NiPeriP ORTEP (50% probability) structure and height of the atoms of the porphyrin core toward its mean plan.

The same assessment can be done with **MyrtP**. It is more difficult to compare together **MyrtP** and **PeriP** as the *meso* substituents are different, another phenomenon (e.g., the anisotropic effect through space due to the π-electrons of the substituents double bond) can affect the β-H chemical shifts. In addition, β-H signal have different multiplicities: broad singlet for **H_2MyrtP**, **NiMyrtP** and **NiPeriP**, broad doublet for **H_2PeriP** and **ZnMyrtP** and finally complex multiplet for **ZnPeriP**.

To try to understand these different features we have performed variable temperature NMR experiments. The spectra obtained show that the signal of the β-H protons always follows the same behaviour (Fig. 3). At high temperature, a singlet is observed, at intermediate temperature there is a splitting (at the first coalescence temperature T_{c1}) in two signals not well resolved, and at low temperature a complicated pattern appears (coalescence temperature T_{c2}). Each of these processes takes place at different temperatures depending on the porphyrin. The observed values of coalescence temperature are summarized in Table 3. For a given metal, **PeriP** has a higher coalescence temperature than **MyrtP**. For a family of porphyrins, the coalescence temperature follows the order Zn>free base>Ni. It is interesting to notice that no other signal on these NMR spectra shows this kind of behaviour. Nevertheless, at very low temperature for **MyrtP** we can observe a splitting of H_1 (already observed for **NiMyrtP**[4]) and a splitting of the N–H protons of the free base in a complex signal. For other ^{1}H NMR signals no splitting or important shift are observed, but there is a broadening of the peaks when the temperature is lowered. This can be partly explained by the increase in the solvent viscosity and the difficulty to obtain homogenous magnetic field at low temperature. For **ZnPeriP** and **NiMyrtP**, only one coalescence temperature can be reached due to the temperature range of the NMR spectrometer, from 200 to

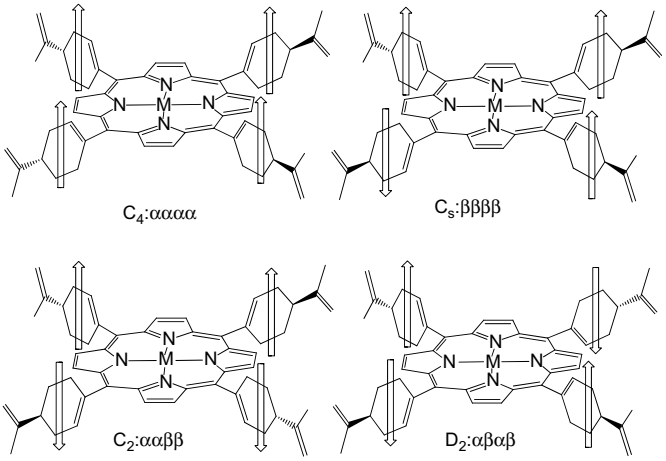

Scheme 2. Representation of the different atropoisomers and symmetries available for *meso*-substituted porphyrins.

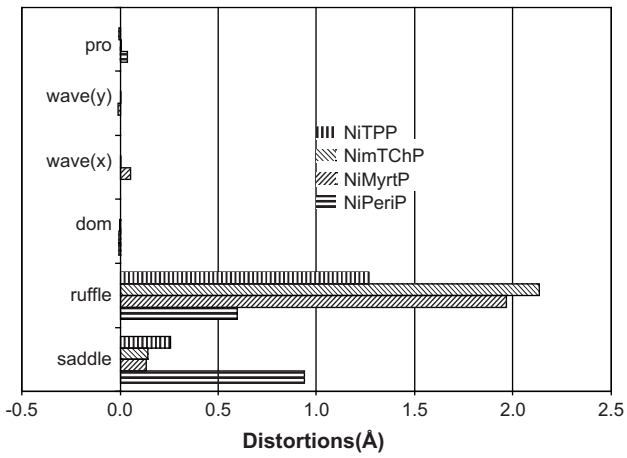

Figure 2. NSD analysis of **NiPeriP**.

Table 2
^{1}H NMR chemical shifts for selected protons

Porphyrin	β-H (ppm)	H_1 (ppm)	NH (ppm)
H_2PeriP	9.30 (d)	6.59	−2.99
H_2MyrtP	9.36 (s)	6.32	−2.70
ZnPeriP	9.42 (m)	6.57	
ZnMyrtP	9.72 (d)	6.45	
NiPeriP	9.17 (s)	6.47	
NiMyrtP	9.17 (s)	6.17	

363 K. To go further into the understanding of these results, we used the Eyring method[21,22] to calculate the activation free energy of each process at the coalescence temperature. The Eyring equation used is the following:

$$\Delta G^{\neq} = 19.14 \times T_c[9.972 + \log(T_c/\delta\nu)] \text{ with } \Delta G^{\neq} \text{ in kJ mol}^{-1}$$

In this equation, T_c (in K) is the coalescence temperature and $\delta\nu$ (in Hz) is the chemical shift difference between the two sites. For the first splitting $\delta\nu$ is calculated from the difference in chemical shifts on the doublet just above T_{c2}. For the second splitting, $\delta\nu$ is calculated on the spectrum registered at the lowest temperature. The results are reported in Table 3. The values of the free energy of rotation[23–26] range from 43.0 to 73.7 kJ mol^{-1}, and the energy difference between the two rotational processes (Tc_1, Tc_2) varies from 2.2 to 14.3 kJ mol^{-1}.

2.3. Discussion

2.3.1. Synthesis

As we know, synthesis of *meso* α,β-unsaturated porphyrins from α,β-unsaturated aldehydes is a difficult challenge.[5] The reactivity of the α,β-unsaturated aldehyde toward the porphyrinogen formation is very weak; several explanations can be proposed. One of them appears if we consider the mechanism of the porphyrinogen synthesis. The proposed mechanism is a succession of pyrrole 1,2 addition on an acid activated aldehyde followed by the pyrrole substitution of the resulting acid activated alcohol. So with α,β-unsaturated aldehyde the first addition can be done either on 1,2 position or on 1,4 position (Scheme 3 path A). In the latter case, the product obtained is not able to lead to the porphyrinogen. Myrtenal for which the position 4 is greatly hindered probably gives less 1,4 addition and consequently a good yield toward porphyrin synthesis. On the opposite (*S*)-(−)-perillaldehyde in which position 4 is not hindered gives more 1,4 addition and a poor porphyrin yield. The same reason can be invoked for 1-cyclohexene-1-carboxaldehyde. For comparison, we tried to achieve porphyrin synthesis starting from 3-cyclohexene-1-carboxaldehyde in which the double bond is not conjugated, and we obtained a yield of 18%. Another argument can be found in the lack of reactivity of 1-cyclopentene-1-carboxaldehyde for porphyrin synthesis. Actually, it is known[27] that α,β-unsaturated imines bearing C5 ring give rise to more 1,4 addition compared to C6 ring, the same statement might be true for aldehydes.

The fact that the yield is better when 1,3-dioxolane derived from the α,β-unsaturated aldehyde is used as starting material is not easy to understand. A first assumption is that hydrolysis of the dioxolane releases slowly the aldehyde, keeping the latter to a low concentration and by this way favouring the porphyrinogen syntheses. But this hypothesis cannot account for the higher reaction kinetics observed with dioxolane (5 times faster). The answer may be found in the dioxolane hydrolysis process, which is easy in acidic medium for the considered molecules. An intermediate of this process is a hemiacetal, possessing ether and alcohol functions. In acidic medium this alcohol can be activated and the pyrrole molecule might react not by addition but by substitution (Scheme 3 path B). By this approach it is perhaps possible to improve and partly overcome the specific poor reactivity of α,β-unsaturated aldehydes towards the porphyrin syntheses. Furthermore, by this protocol, it is possible to greatly diminish (by 2.5 times) the quantity of solvent necessary for these porphyrin syntheses.

2.3.2. Dynamic behaviour of the porphyrins

Variable temperature ^{1}H NMR spectra show that α,β-unsaturated porphyrins present two consecutive and distinct dynamic process, having activation free energies near 50–70 kJ mol^{-1}. For *meso*-substituted porphyrins, several dynamic phenomena can exist: rotation of the substituent around the *meso* C–C bond, N–H bond tautomerism, or inversion of the porphyrin core distortion. This last process has been proposed by Marchon[4] to account for the splitting of H_1 at very low temperature in **NiMyrtP**. This assessment is made on the basis of the work of Eschenmoser[28] on the octaethyl porphyrin for which an activating energy of 50.6 kJ mol^{-1} for the porphyrin core inversion is found. Nevertheless, a more recent work of Kleinpeter[29] on dithianyl porphyrins proves that for less hindered *meso*-substituted porphyrin, this process possesses

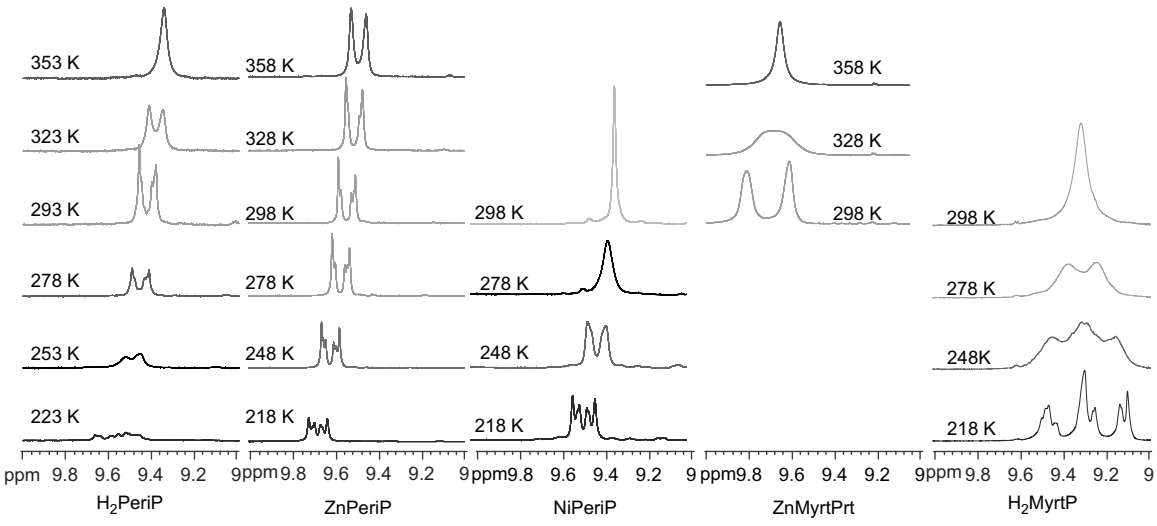

Figure 3. Variable temperature ^{1}H NMR of the β-H region registered for all studied porphyrins (for **NiMyrtP**, see Ref. 4).

Table 3
Coalescence temperature and thermodynamic data obtained from variable temperature NMR experiments and theoretical simulations

Porphyrin	T_c (K)	$\Delta\nu$ (Hz)	$\Delta G^{\neq}$ (kJ mol^{-1})	Theoretical minimum energy (eV)	Theoretical maximum energy (eV)	E_a (kJ mol^{-1})
H_2PeriP	T_{c1}=343	30	72.3	−747.12	−745.92	B_1=117.5
	T_{c2}=273	20	58.0	−747.14	−746.31	B_2=80.1
H_2MyrtP	T_{c1}=288	75	58.0	−745.43	−744.52	B_1=87.1
	T_{c2}=258	20	54.6	−770.17	−744.60	B_2=80.0
ZnPeriP	T_{c1} nd	nd	nd	−770.17	−769.18	B_1=95.6
	T_{c2}=338	12	73.7	−770.17	−769.21	B_2=93.3
ZnMyrtP	T_{c1}=333	82	67.3	−768.38	−767.53	B_1=89.4
	T_{c2}=298	10	65.1	−768.46	−767.57	B_2=85.5
NiPeriP	T_{c1}=278	34	57.8	−774.14[b]	−773.16[b]	B_1=96.2
	T_{c2}=298	10	53.3	−774.15[b]	773.46[b]	B_2=67.0
				−774.17[a]	−773.12[a]	B_1=103.1
				−774.19[a]	−773.19[a]	B_2=96.1
NiMyrtP	T_{c1}=213	53	43.0	−772.57	−772.11	B_1=52.8
	T_{c2} nd	nd	nd	−772.66	−772.11	B_2=52.3

[a] Calculated from conditions **A**.
[b] Calculated from conditions **B** (see text).

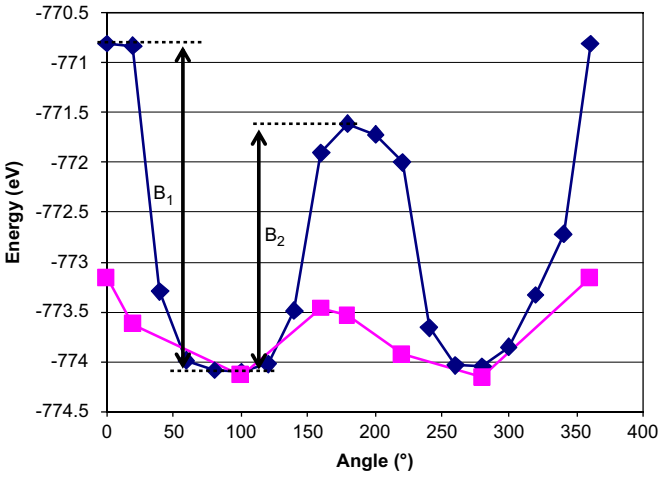

Figure 4. Evolution of the **ZnPeriP** energy as a function of the dihedral angle C_α–C_{meso}–C_6–C_1: ◆ without geometry optimization, ■: with geometry optimisation.

a lower activation energy, i.e., around 6 kJ mol^{-1}. Consequently, this low energetic process cannot be reached with our NMR experiments. Another key point to reject this assumption is that even for the flat zinc(II) porphyrins where no inversion of the porphyrin core distortion is possible, we observe the same behaviour. The N–H bond tautomerism deals only for free base porphyrins, and we observe the same behaviour for the zinc and the nickel complexes. Furthermore, this tautomerism becomes slow toward the NMR time scale at lower temperatures.[30,31] For **H_2MyrtP**, the complex signal observed at low temperature is different from the two singlets expected if the N–H tautomerism is involved. So the explanation for these two dynamic processes needs to be linked to the substituents motion. Cyclohexyl compounds are well known to have favoured conformations (chair and boat) in equilibrium. The same behaviour can be found in cyclohexene compounds, however, with myrtenal this kind of phenomenon cannot be involved due to the rigidity of the molecule. Even in the case of perillaldehyde, as the isopropene is more stable in an equatorial conformation, it seems difficult for this process to occur. Besides, all the signals of the (*S*)-perillyl substituent remained unchanged over the studied temperature range. Consequently, the dynamic behaviour of *meso* α,β-unsaturated porphyrins results from a particular process, occurring during the substituent rotation around the *meso* C–C bond.

Theoretical calculations give us an estimate of the total energy changes of the molecule as function of the rotation of the substituent (see Section 4.4 for the detailed energetic analyses that were carried out). For the six porphyrins studied we obtained the same pattern (Fig. 4), when exploring the total energy versus the rotational dihedral angle of the substituent. Two maxima and two minima can be found, each of them possessing distinct energies (Table 3). So if at high temperature, the substituent can freely rotate, when the temperature decreases and reaches T_{c1}, it is no more able to pass the higher rotational level (B_1), then the spinning is partly blocked giving rise to a splitting of the pyrrolic protons' NMR signal into two broad singlets. For a lower temperature (T_{c2}), it is no more possible for the substituent to go through the second rotational barrier (B_2) and in NMR we observe a complex signal. We can notice that for a given substituent at low temperature as in the solid state, only two orientations are possible: α or β. Consequently only four atropoisomers of distinct symmetry can exist (Scheme 3): αααα, βααα, ααββ and αβαβ. For each of these atropoisomers a specific multiplicity of the pyrrolic protons is expected, respectively, one singlet, four doublets, two singlets and two doublets, finally two singlets. The two β-H signals observed at an intermediate temperature correspond to a random D_2 symmetry and to a αβαβ atropoisomer as observed on the crystal structure. At lower temperature, as the substituent can be trapped randomly in the two energetic minima, a mixture of several atropoisomers is obtained and gives an intricate pattern on the ^{1}H NMR spectrum. As atropoisomers are not equivalent in the NMR point of view, this also explains the splitting of the N–H signals in **H_2MyrtP**. By calculating the activation energy between the lowest minima and the two surrounding maxima, we notice a good agreement between experimental and theoretical values, especially for the second rotational barriers (**B_2**) for which theoretical and experimental results follow the same trend with respect to the porphyrin.

For a given porphyrin (**PeriP** or **MyrtP**), the observation that the nickel complexes have the lowest activation energy to rotate the *meso* substituents, followed by the free base porphyrins and finally the zinc complexes, is well known and relates directly to the distortion of the porphyrin core.[17,32–35] If we compare **PeriP** and **MyrtP** family, the latter possesses the lowest free energy to rotate the *meso* substituents. But if we compare the bulkiness of the substituents, myrtenal is bigger and more rigid than perillaldehyde. Nevertheless, as we have proved in the characterization part of this manuscript, the bulkiness of the myrtenal leads to more distorsions for **MyrtP**, and consequently, facilitates the substituent rotation. This means that even in the case of very bulky substituents, a very distorted porphyrin core can allow a low rotational barrier.

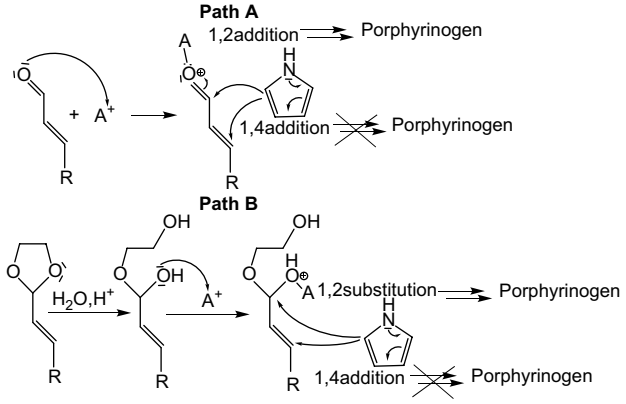

Scheme 3. proposed mechanism for the porphyrins synthesis: path A: starting from α,β-unsaturated aldehyde, path B: starting from 1,3-dioxolane of α,β-unsaturated aldehyde.

To go further in the discussion concerning **NiPeriP**, our X-ray structure shows that in the solid state its mean distortion mode is saddled. But this can result from the packing of the porphyrins in the crystal. To have a better view of this point, we calculated the rotational activation energy by two different ways (see Section 4.4). In the first case (**A**), we started from the X-ray structure of **NiPeriP**, followed by a full geometry optimization. In the second case (**B**), we used the X-ray structure of **NiMyrtP**, replaced the myrtenal substituents by perillaldehyde ones and completed the same full optimization. In these two optimized structures, the porphyrin distortion stays in the starting distortion mode, i.e., saddled for **A** (angles C_α–N–N–C_α=13.48° and N–Ni–N=177.9°) and ruffled for **B** (angles C_α–N–N–C_α=39.47° and N–Ni–N=178.49°), however, for the latter, the distortion is weaker. The initial distortion mode is retained through optimization, because a local minimum is found close to the starting geometry (see Section 4.4). The results obtained with **B** are in a better agreement compared to the experimental values, than those for **A** (particularly for $\mathbf{B_2}$). This can be an indication of a change in the predominant distortion mode of **NiPeriP** in solution from saddled to ruffled, and an increase of the distortion. This point is in good agreement with the assessment that the distortion observed in the solid state is related to the packing of the porphyrin in the crystal lattice, and does not exist in solution. This difference between solid and solution is already observed for other nickel(II) porphyrins.[16]

Finally it is interesting to compare the free activation energies obtained for the *meso* α,β-unsaturated porphyrins studied here with those obtained for other cyclic *meso*-substituted porphyrins (Table 4). **TPP**,[32–35] **H_2TPPOMe**,[36] **TChP**[17,37] and dithianyl porphyrins[29] possess only one observable coalescence temperature linked to the rotation of the substituting moiety. This can be related to the symmetry of these substituents, so the two rotational barriers involved during the spinning are probably of equal energy. For *meso* α,β-unsaturated porphyrins studied here, the substituents are unsymmetrical, and β-H atoms can be close to the sp^2 or the sp^3 carbon atom of the substituent. Moreover, in a general way the porphyrin core distortion, even if weak, decreases the porphyrin symmetry, especially during the crossing of the activation barrier. So these two losses of symmetry can result in a splitting of the two rotational barriers and consequently lead to two temperatures of coalescence. This may also explain why the rotational barriers are higher for these porphyrins compared to **TPP** or **TChP**. Only dithianyl porphyrins show activation energy of the same level but the rotation is slowed down by two bulky sulfur atoms located near the β-pyrrolic protons.

Table 4
Comparison of the free energy of activation for various porphyrins

Porphyrin	$\Delta G^{\neq}$ (kJ mol^{-1})	$\Delta G^{\neq}$ (kJ mol^{-1})	Reference
H_2PeriP	72.3	58	This work
H_2MyrtP	58	54.6	This work
H_2TPPOMe[a]	45	—	36
H_2P_1[a]	61.8	—	29
H_2P_2[a]	57.3	—	29
H_2P_3[a]	59.7	—	29
ZnPeriP	—	73.7	This work
ZnMyrtP	67.3	65.1	This work
ZnmTChP[a]	50.2		17
NiPeriP	57.8	53.3	This work
NiMyrtP	43.0	—	This work and Ref. 4
NimTChP[a]	40.1	—	17
NiP_1[a]	47.6	—	29

H_2TPPOMe: 5,10,15,20-(3-methoxyphenyl) porphyrin, **P_1**: 5-dithianyl, 10,20-phenyl porphyrin, **P_2**: 5,15-dithianyl, 10,20-phenyl porphyrin, **P_3**: 5-dithianyl, 10,15,20-phenyl porphyrin.
[a] Only one coalescence temperature.

3. Conclusion

From the synthetic point of view, the reactivity of α,β-unsaturated aldehydes is very limited toward the porphyrins formation. To date no easy and general procedure is available, this study gives new keys for such synthesis. The original dynamic behaviour of these porphyrins has been experimentally and theoretically studied. As we know that the atropoisomer composition is important for the catalytic properties of these molecules, this particular behaviour points out the interest of expanding the studies on *meso* α,β-unsaturated porphyrins.

4. Experimental section

4.1. General

All solvents and reagents were of the highest quality available and used as received unless noted otherwise. (1*R*)-Myrtenal, (*S*)-(−)-perillaldehyde, 1-cyclohexene-1-carboxaldehyde, 3-cyclohexene-1-carboxaldehyde, TFA, ethylene glycol, benzene, tartaric acid, anhydrous magnesium sulfate and $BF_3{\cdot}Et_2O$ were purchased from Sigma Aldrich. 1,3-Dioxolanes of α,β-unsaturated aldehydes are synthesized following a published procedure.[38]

4.2. Synthesis

4.2.1. 2-(Cyclopenten-1-yl)-1,3-dioxolane

This compound was synthesised in 89% yield following the published procedure.[38] ^{1}H NMR ($CDCl_3$, 200 MHz): δ=1.92 (m, 2H), 2.38 (m, 4H), 3.90–4.02 (m, 4H), 5.43 (s, 1H), 5.90 (br s, 1H).

4.2.2. 2-(Cyclohexen-1-yl)-1,3-dioxolane

This compound was synthesised in 90% yield following the published procedure.[38] ^{1}H NMR ($CDCl_3$, 200 MHz): δ=1.55 (m, 4H), 1.86 (m, 2H), 2.21 (m, 2H), 3.42–3.56 (m, 4H), 5.14 (s, 1H), 5.87 (m, 1H).

4.2.3. 5,10,15,20-Tetra-cyclohex-1-enyl-porphyrin

In a bottle shielded from light, 2.85 mL (25 mmol) of 2-cyclohexenyl-1,3-dioxolane and 0.7 mL of pyrrole (10 mmol) were dissolved in 1 L of chloroform (stabilized with 1% ethanol) and degassed with argon. TFA (0.77 mL, 10 mmol) was added after 10 min. The solution was stirred under argon for 6 h. Then the solution was oxidized by adding 1.7 g (7.4 mmol) of DDQ. After stirring for 30 min, the solution was concentrated twice and filtered through a pad of basic alumina, CH_2Cl_2 was used to elute the porphyrin. The porphyrin was further purified by column chromatography, on basic alumina, using CH_2Cl_2/pentane (50:50) mixture as eluent. The porphyrin was obtained as a purple solid (63 mg, 4%). MS (ESI): 631.7 $[M-H]^+$. HRMS (ESI): 631.37915 uma $[M-H]^+$; theoretical for $C_{44}H_{47}N_4$: 631.37952 uma. UV/vis (CH_2Cl_2, λ_{max}/nm (ε/mol^{-1} L cm^{-1})): 415 (2.5×10^5), 510 (9.3×10^3), 546 (3.8×10^3), 586 (2.7×10^3), 644 (1.2×10^3). ^{1}H NMR ($CDCl_3$, 200 MHz): δ=−3.00 (s, 2H), 2.23 (m, 16H), 2.78 (m, 8H), 3.21 (m, 8H), 6.55 (m, 4H), 9.31 (s, 8H). ^{13}C NMR ($CDCl_3$, 400 MHz): δ=22.71, 24.02, 26.37, 37.65, 121.88, 129.58, 128.32, 132.79, 139.47.

4.2.4. 5,10,15,20-Tetra-cyclohex-3-enyl-porphyrin

3-Cyclohexene-1-carboxaldehyde (1.15 mL, 1.0 mmol) and pyrrole (0.70 mL, 1.0 mmol) were dissolved in 1 L of chloroform (stabilized with 1% ethanol). The solution was shielded from light and 0.77 mL (10 mmol) of TFA was added after 10 min. The solution was stirred under argon for 24 h. Then the solution was oxidised by adding 1.7 g (7.4 mmol) of DDQ. After stirring for 30 min, the solution was concentrated twice and filtered through a pad of basic alumina, CH_2Cl_2 was used to elute the porphyrin. The porphyrin

was further purified by recrystallization in methylene chloride/pentane mixture. The porphyrin was obtained as purple crystals (270 mg, 18%). MS (ESI): 631.6 $[M-H]^+$. HRMS (ESI): 631.37903 uma $[M-H]^+$; theoretical for $C_{44}H_{47}N_4$: 631.37952 uma. UV/vis (CH_2Cl_2, λ_{max}/nm (ε/mol^{-1} L cm^{-1})): 423 (3.3×10^5), 524 (1.2×10^4), 561 (6.8×10^3), 602, 659. ^{1}H NMR ($CDCl_3$, 200 MHz): δ=−1.70 (s, 2H), 2.26 (m, 12H), 3.18 (m, 8H), 3.72 (m, 8H), 5.05 (m, 4H), 6.15 (m, 4H), 9.42 (s, 8H). ^{13}C NMR ($CDCl_3$, 400 MHz): δ=27.8, 34.4, 38.3, 42.3, 122.1, 127.7, 127.8, 129.2.

4.2.5. 5,10,15,20-Tetrakis-((S)-4-isopropenyl-cyclohex-1-enyl)-porphyrin, ***H$_2$PeriP***

1,3-Dioxolane (3.8 mL) derived from perillaldehyde (25 mmol) and pyrrole (0.7 mL, 10 mmol) were dissolved in 1 L of chloroform degassed with argon (stabilized with 1% ethanol). The solution was shielded from light and 0.77 mL (10 mmol) of TFA was added after 10 min. The solution was stirred under argon for 6 h. Then the solution was oxidised by adding 1.7 g (7.4 mmol) of DDQ. After stirring for 30 min, the solution was concentrated twice and filtered through a pad of basic alumina, CH_2Cl_2 was used to elute the porphyrin. The porphyrin was further purified by column chromatography, on basic alumina, using CH_2Cl_2/pentane (50:50) mixture as eluent. The porphyrin was obtained as a purple solid (117 mg, 6%). MS (ESI): 791.8 $[M-H]^+$. HRMS (ESI): 791.50470 uma $[M-H]^+$; theoretical for $C_{56}H_{63}N_4$: 791.50472 uma. UV/vis (CH_2Cl_2, λ_{max}/nm (ε/mol^{-1} L cm^{-1})): 416 (2.7×10^5), 444 (8.4×10^4), 513, 546, 589, 647. ^{1}H NMR ($CDCl_3$, 200 MHz): δ=−2.99 (s, 2H), 2.06 (s, 12H), 2.36 (m, 8H), 2.78 (m, 8H), 2.86 (m, 4H), 3.30 (m, 8H), 5.10 (d, 8H), 6.59 (s, 4H), 9.30 (d, 8H). ^{13}C NMR ($CDCl_3$, 400MHz): δ=21.23, 28.75, 29.70, 31.66, 37.78, 40.99, 109.3, 121.47, 129.80, 132.20, 139.16, 149.78.

4.2.6. Nickel complex of 5,10,15,20-tetrakis-((S)-4-isopropenyl-cyclohex-1-enyl)-porphyrin, ***NiPeriP***

H$_2$PeriP (20 mg) was dissolved in 20 mL of $CHCl_3$, 10 mg of nickel chloride dissolved in a minimum amount of ethyl alcohol was added, and the mixture was refluxed 18 h. After removal of the solvent, the product was dissolved in $CHCl_3$ and washed three times with water. The solvent was dried over sodium sulfate and removed. The porphyrin was further purified by column chromatography on basic alumina, using CH_2Cl_2/pentane (50:50) mixture as eluent. The porphyrin was obtained as a red solid with a yield around 80%. MS (ESI): 846.7 $[M^{\bullet}]^+$. UV/vis (CH_2Cl_2, λ_{max}/nm (ε/mol^{-1} L cm^{-1})): 413 (1.4×10^5), 525 (9.4×10^4), 647. ^{1}H NMR ($CDCl_3$, 400 MHz): δ=2.00 (br s, 12H), 2.22 (m, 8H), 2.65 (m, 4H), 2.77 (m, 8H), 3.05 (br s, 8H), 4.96 (s, 4H), 5.10 (s, 4H), 6.47 (br s, 4H), 9.17 (s, 8H$_\beta$). ^{13}C NMR ($CDCl_3$, 400 MHz): δ=21.17, 28.58, 31.52, 36.66, 40.89, 109.22, 120.37, 130.82, 131.57, 137.83, 141.55, 149.72.

4.2.7. Zinc complex of 5,10,15,20-tetrakis-((S)-4-isopropenyl-cyclohex-1-enyl)-porphyrin, ***ZnPeriP***

The same procedure as for **NiPeriP** was applied, using zinc acetate instead of nickel chloride. MS (ESI): 853.7 $[M-H]^+$. HRMS (ESI): 853.41819 uma $[M-H]^+$; theoretical for $C_{56}H_{61}N_4Zn$: 853.41822 uma. UV/vis (CH_2Cl_2, λ_{max}/nm (ε/mol^{-1} L cm^{-1})): 417 (2.9×10^5), 546 (1.4×10^4), 586. ^{1}H NMR ($CDCl_3$, 400 MHz): δ=2.06 (s, 12H) 2.32 (m, 8H), 2.74 (m, 4H), 2.82 (m, 8H), 3.33 (m, 8H), 5.00 (s, 4H), 5.19 (s, 4H), 6.57 (br s, 4H), 9.42 (m, 8H$_\beta$). ^{13}C NMR ($CDCl_3$, 400 MHz): δ=21.25, 28.82, 29.70, 31.71, 37.92, 41.05, 109.26, 122.58, 130.56, 131.73, 139.65, 149.89.

4.2.8. meso-[Tetra-(1R)-apopinen-2-yl]-porphyrin, ***H$_2$MyrtP***

Myrtenal (3.12 mL, 25 mmol) and pyrrole (0.7 mL, 10 mmol) were dissolved in 1 L of chloroform (stabilized with 1% ethanol) degassed with argon. The solution was shielded from light, and 0.77 mL (10 mmol) of TFA was added after 10 min. The solution was stirred under argon for 15 h. Then the solution was oxidised by adding 1.7 g (7.4 mmol) of DDQ. After stirring for 30 min, the solution was concentrated twice and filtered through a pad of basic alumina, CH_2Cl_2 was used to elute the porphyrin. The porphyrin was further purified by column chromatography, on basic alumina, using CH_2Cl_2/pentane (50:50) mixture as eluent. The porphyrin was obtained as a purple solid (330 mg, 17%). Crystals are obtained from a methanol/dichloromethane mixture. MS (ESI): 791.8 $[M-H]^+$. UV/vis (CH_2Cl_2, λ_{max}/nm): 427 (ε=3.31×10^5 mol^{-1} L cm^{-1}), 528, 568, 603, 664. ^{1}H NMR ($CDCl_3$, 200 MHz): δ=−2.70 (s, 2H), 1.54 (s, 12H), 1.68 (s, 12H), 2.33 (d, J=8.6 Hz, 4H), 2.58 (m, 4H), 3.06 (m, 12H), 3.45 (m, 4H), 6.39 (m, 4H), 9.36 (br s, 8H). ^{13}C NMR ($CDCl_3$, 200 MHz): δ=22.4, 26.9, 33.1, 33.8, 39.1, 40.6, 54.3, 122.4, 130.1, 130.8, 146.0, 149.0.

4.2.9. Nickel complex of meso-[tetra-(1R)-apopinen-2-yl]-porphyrin, ***NiMyrtP***

The same procedure as for **NiPeriP** was applied. Crystals was obtained from a acetonitrile/chloroform mixture. MS (ESI): 848 $[M-H]^+$. UV/vis (CH_2Cl_2, λ_{max}/nm): 425 (ε=2.19×10^5 mol^{-1} L cm^{-1}), 541, 580. ^{1}H NMR ($CDCl_3$, 200 MHz): δ=1.41 (12H, s), 1.42 (12H, s), 2.14 (4H, d, J=8.7 Hz), 2.45 (4H, m), 2.86 (12H, m), 3.03 (4H, m), 6.17 (4H, m), 9.17 (8H, m). ^{13}C NMR ($CDCl_3$, 200 MHz): δ=22.0, 26.6, 32.8, 33.4, 38.8, 40.7, 52.9, 119.4, 128.9, 131.3, 141.1, 147.3.

4.2.10. Zinc complex of meso-[tetra-(1R)-apopinen-2-yl]-porphyrin, ***ZnMyrtP***

The same procedure as for **ZnPeriP** was applied. Crystals were obtained from a methanol/dichloromethane mixture. MS (ESI): 853.4 $[M-H]^+$. UV/vis (CH_2Cl_2, λ_{max}/nm): 420, 559, 603. ^{1}H NMR ($CDCl_3$, 200 MHz): δ=1.55 (s, 12H), 1.74 (s, 12H), 2.38 (d, J=8.7 Hz, 4H), 2.60 (m, 4H), 3.04 (m, 12H), 3.46 (m, 4H), 6.38 (m, 4H), 9.44 (br s, 4H), 9.61 (br s, 4H). ^{13}C NMR ($CDCl_3$, 200 MHz): δ=22.3, 26.8, 33.0, 33.8, 39.0, 40.6, 54.3, 122.2, 130.0, 130.8, 149.2.

4.3. Spectroscopic measurements

Electronic absorption spectra were recorded on a Hewlett Packard HP 89090A or 8452A diode array spectrophotometer. ^{1}H and ^{13}C NMR spectra were recorded on a Bruker AC 200, Bruker Avance 400, 500 or Varian 400 spectrometers with a characteristic absorption of the solvent as internal reference. Standard spectra were recorded in $CDCl_3$, variable temperature experiments were carried out using deuteriated toluene. Electrospray ionization mass spectra were obtained with a LCQ Finnigan Thermoquest ESI source spectrometer with an ion trap and an octupolar analyzer or a LTQ spectrometer from Thermo Electron. HRMS were recorded on a LXQ spectrometer from Thermo Electron.

4.4. Computational details

All calculations have been carried out in the Kohn-Sham formalism within the Density Functional Theory framework, using Amsterdam Density Functional (ADF) 2006.[39–41] The basis sets were made of Slater-type orbital double-zeta functions including one polarization function for H, C and N. Frozen cores were used for C, N (1s) and 3d metal (1s–3p). The exchange and correlation potentials were, respectively, the Becke 88 and Perdew 86[42,43] functionals. Both metal ion (Zn^{2+} and Ni^{2+}) complexes with porphyrins have a singlet ground state[44] and thus all systems were closed-shell. Total bonding energies were calculated using the usual procedure from the generalized transition state from Ziegler.[45]

The starting geometries were derived from crystallographic structures. The free base **H$_2$PeriP** came from a low resolution (see Supplementary data) X-ray crystallographic structure obtained by us, and the Zn^{2+} complex was generated from this structure. The MyrtP analog was obtained by changing perillyl substituents into

myrtenyl ones using the facilities of the Chem3D modeling software.[46] This procedure allowed thus to get the starting structures for **PeriP** and **MyrtP** free base and Zn species. The **NiMyrtP** was obtained from the X-ray crystallographic structure.[4] For **NiPeriP**, two starting structures were used. One was derived from **NiMyrtP** by changing the peripheral groups using Chem3D software. The other one came directly from the X-ray structure obtained by us. All these starting structures were then fully optimized using ADF, using the default geometric convergence criteria.[39]

Then we used the same procedure to calculate the conformational barriers of all systems. Starting from the initially fully optimized structure, a fast scan of the energy curve was carried out by computing single points energies on geometries generated by rotating one of the peripheral group, by steps of 20° in a 360° range for the corresponding dihedral angle. From these conformational profiles, we extracted structures around each minimum and maximum and submitted them to a full geometry optimization, except for the dihedral angle that was kept fixed. We thus calculated the energetic barriers between maxima and minima from these structures. As such, these energies correspond to enthalpic terms. The entropy changes have not been evaluated, as we assume that the changes in entropy between two conformers are negligible. The solvent was not taken into account in our calculations. Actually, one series of calculations was performed on the **ZnPeriP** species including toluene solvent through the Polarizable Continuum Model (COSMO in ADF). We have not observed any change in the structures and energy barriers between the gas phase and solvent results.

The accuracy on energy values, i.e., the minimum difference, which can be considered as being significant, is ca. 5×10^{-2} eV.

It should be mentioned that the geometries resulting from the first full optimization are generally close to the starting ones. If the initial structure exhibits a particular distorsion of the central core, the optimization process is able to find the equilibrium point, which is closest to this distorsion, and will not be able to explore other ones. This is true for instance in the case of **NiPeriP**, where two starting structures were used (as abovementioned), giving after complete optimizations, two differently distorted porphyrins.

Acknowledgements

A.C. whishes to thank funding from the European Community under the FP6—Marie Curie Host Fellowships for Early Stage Research Training (EST) 'CHEMTRONICS' Contract Number MEST-CT-2005-020513. We thank Eric Genin from Thermo Electron France for providing us HRMS analysis.

Supplementary data

Structure of **NiPeriP** is deposited to the CCDC under the number 688686 and available upon request. Yield of the synthesis of **H_2PeriP** in different conditions, full ^{1}H NMR spectrum of the variable temperature experiment, CIF file of the low resolution **H_2PeriP** structure used as starting point for calculation, and Cartesian coordinates of the optimized structure are available as electronic Supplementary data. Supplementary data associated with this article can be found in the online version, at doi:10.1016/j.tet.2008.09.009.

References and notes

1. Rose, E.; Andrioletti, B.; Zrig, S.; Quelquejeu-Ethève, M. *Chem. Soc. Rev.* **2005**, *34*, 573–583.
2. Gazeau, S.; Pécaut, J.; Haddad, R.; Shelnutt, J. A.; Marchon, J. C. *Eur. J. Inorg. Chem.* **2002**, 2956–2960.
3. Song, Y.; Haddad, R. E.; Jia, S. L.; Hok, S.; Olmstead, M. M.; Nurco, D. J.; Schore, N. E.; Zhang, J.; Ma, J. G.; Smith, K. M.; Gazeau, S.; Pécaut, J.; Marchon, J. C.; Medforth, C. J.; Shelnutt, J. A. *J. Am. Chem. Soc.* **2005**, *127*, 1179–1192.
4. Veyrat, M.; Maury, O.; Faverjon, F.; Over, D. E.; Ramasseul, R.; Marchon, J. C.; Turowska-Tyrk, I.; Scheidt, W. R. *Angew. Chem., Int. Ed. Engl.* **1994**, *33*, 220–223.
5. Lindsey, J. S.; Schreiman, I. C.; Hsu, H. C.; Kearney, P. C.; Marguerettaz, A. M. *J. Org. Chem.* **1987**, *52*, 827–836.
6. Anderson, H. L. *Tetrahedron Lett.* **1992**, *33*, 1101–1104.
7. Anderson, H. L.; Wylie, A. P.; Prout, K. *J. Chem. Soc., Perkin Trans. 1* **1998**, 1607–1611.
8. Caselli, A.; Gallo, E.; Ragaini, F.; Ricatto, F.; Abbiati, G.; Cenini, S. *Inorg. Chim. Acta* **2006**, *359*, 2924–2932.
9. Horn, S.; Sergeeva, N.; Senge, M. O. *J. Org. Chem.* **2007**, *72*, 5414–5417.
10. Milgrom, L. R.; Rees, R. D.; Yahioglu, G. *Tetrahedron Lett.* **1997**, *38*, 4905–4908.
11. Milgrom, L. R.; Yahioglu, G. *Tetrahedron Lett.* **1995**, *36*, 9061–9064.
12. Milgrom, L. R.; Yahioglu, G. *Tetrahedron Lett.* **1996**, *37*, 4069–4072.
13. Proess, G.; Pankert, D.; Hevesi, L. *Tetrahedron Lett.* **1992**, *33*, 269–272.
14. Geier, G. R.; Ciringh, Y.; Li, F. R.; Haynes, D. M.; Lindsey, J. S. *Org. Lett.* **2000**, *2*, 1745–1748.
15. Hevesi, L.; Renard, M.; Proess, G. *J. Chem. Soc., Chem. Commun.* **1986**, 1725–1727.
16. Jentzen, W.; Simpson, M. C.; Hobbs, J. D.; Song, X.; Ema, T.; Nelson, N. Y.; Medforth, C. J.; Smith, K. M.; Veyrat, M.; Mazzanti, M.; Ramasseul, R.; Marchon, J. C.; Takeuchi, T., III; Goddard, W. A.; Shelnutt, J. A. *J. Am. Chem. Soc.* **1995**, *117*, 11085–11097.
17. Veyrat, M.; Ramasseul, R.; Turowska-Tyrk, I.; Scheidt, W. R.; Autret, M.; Kadish, K. M.; Marchon, J. C. *Inorg. Chem.* **1999**, *38*, 1772–1779.
18. Richard, P.; Rose, E.; Boitrel, B. *Inorg. Chem.* **1998**, *37*, 6532–6534.
19. Jentzen, W.; Song, X. Z.; Shelnutt, J. A. *J. Phys. Chem. B* **1997**, *101*, 1684–1699.
20. Haddad, R. E.; Gazeau, S.; Pecaut, J.; Marchon, J. C.; Medforth, C. J.; Shelnutt, J. A. *J. Am. Chem. Soc.* **2003**, *125*, 1253–1268.
21. Oki, M. *Applications of Dynamic NMR Spectroscopy to Organic Chemistry*; Deerfield Beach: Florida, USA, 1985; Vol. 4.
22. Sandström, J. *Dynamic NMR spectroscopy*; Academic: London, 1982.
23. Boitrel, B.; Lecas, A.; Renko, Z.; Rose, E. *New J. Chem.* **1989**, *13*, 73–99.
24. Rose, E.; Quelquejeu, M.; Pochet, C.; Julien, N.; Kossanyi, A.; Hamon, L. *J. Org. Chem.* **1993**, *58*, 5030–5031.
25. Rose, E.; Cardon-Pilotaz, A.; Quelquejeu, M.; Bernard, N.; Kossanyi, A.; Desmazières, B. *J. Org. Chem.* **1995**, *60*, 3919–3920.
26. Rose, E.; Quelquejeu, M.; Pandian, R. P.; Lecas-Nawrocka, A.; Vilar, A.; Ricard, G.; Collman, J. P.; Wang, Z.; Straumanis, A. *Polyhedron* **2000**, *19*, 581–586.
27. Rossiter, B. E.; Swingle, N. M. *Chem. Rev.* **1992**, *92*, 771–808.
28. Waditschatka, R.; Kratky, C.; Jaun, B.; Heinzer, J.; Eschenmoser, A. *J. Chem. Soc., Chem. Commun.* **1985**, 1604–1607.
29. Wacker, P.; Dahms, K.; Senge, M. O.; Kleinpeter, E. *J. Org. Chem.* **2007**, *72*, 6224–6231.
30. Gust, D.; Roberts, J. D. *J. Am. Chem. Soc.* **1977**, *99*, 3637–3640.
31. Storm, C. B.; Teklu, Y. *J. Am. Chem. Soc.* **1972**, *94*, 1745–1747.
32. Bonnet, J. J.; Eaton, S. S.; Eaton, G. R.; Holm, R. H.; Ibers, J. A. *J. Am. Chem. Soc.* **1973**, *95*, 2141–2149.
33. Eaton, S. S.; Eaton, G. R. *J. Am. Chem. Soc.* **1977**, *99*, 6594–6599.
34. Eaton, S. S.; Fishwild, D. M.; Eaton, G. R. *Inorg. Chem.* **1978**, 1542–1545.
35. Laurie, A.; Shroyer, W.; Lorbereau, C.; Eaton, S. S.; Eaton, G. R. *J. Org. Chem.* **1980**, *45*, 4296–4302.
36. Crossley, M. J.; Field, L. D.; Forster, A. J.; Harding, M. M.; Sternhell, S. *J. Am. Chem. Soc.* **1987**, *109*, 341–348.
37. Veyrat, M.; Ramasseul, R.; Marchon, J. C.; turowska-Tyrk, I.; Scheidt, W. R. *New J. Chem.* **1995**, *19*, 1199–1202.
38. Lu, T. J.; Yang, J. F. F.; Sheu, L. J. *J. Org. Chem.* **1995**, *60*, 2931–2934.
39. Baerends, E. J. ADF 2006.01. SCM, Theoretical Chemistry; Vrije Universiteit: Amsterdam, The Netherlands, http://www.scm.com.
40. Guerra, C. F.; Snijders, J. G.; Velde, G. t.; Baerends, E. J. *Theor. Chem. Acc.* **1998**, *99*, 391–403.
41. Velde, G. t.; Bickelhaupt, F. M.; Gisbergen, S. J. A.; vGuerra, C. F.; Baerends, E. J.; Snijders, J. G.; Ziegler, T. *J. Comput. Chem.* **2001**, *22*, 931–967.
42. Becke, A. *Phys. Rev. A* **1988**, *38*, 3098–3100.
43. Perdew, J. P. *Phys. Rev. B* **1986**, *33*, 8822–8824.
44. Liao, M. S.; Scheiner, S. *J. Chem. Phys.* **2002**, *117*, 205–219.
45. Ziegler, T.; Rauk, A. *Theor. Chim. Acta* **1977**, *46*, 1–10.
46. Chem3D Ultra 10.0, CambridgeSoft, www.cambridgesoft.com.